Bioorganic & Medicinal Chemistry 19 (2011) 861–870

Contents lists available at ScienceDirect

Bioorganic & Medicinal Chemistry

journal homepage: www.elsevier.com/locate/bmc

Synthesis and in vivo evaluation of ^{18}F-fluoroethyl GF120918 and XR9576 as positron emission tomography probes for assessing the function of drug efflux transporters

Kazunori Kawamura [a,*], Tomoteru Yamasaki [a], Fujiko Konno [a], Joji Yui [a], Akiko Hatori [a], Kazuhiko Yanamoto [a], Hidekatsu Wakizaka [b], Masanao Ogawa [a,c], Yuichiro Yoshida [a,c], Nobuki Nengaki [a,c], Toshimitsu Fukumura [a], Ming-Rong Zhang [a]

[a] Department of Molecular Probes, Molecular Imaging Center, National Institute of Radiological Sciences, 4-9-1 Anagawa, Inage-ku, Chiba 263-8555, Japan
[b] Department of Biophysics, Molecular Imaging Center, National Institute of Radiological Sciences, 4-9-1 Anagawa, Inage-ku, Chiba 263-8555, Japan
[c] SHI Accelerator Service Ltd, 1-17-6 Osaki, Shinagawa-ku, Tokyo 141-0032, Japan

ARTICLE INFO

Article history:
Received 6 October 2010
Revised 1 December 2010
Accepted 2 December 2010
Available online 5 December 2010

Keywords:
Positron emission tomography (PET)
Fluorine-18
P-Glycoprotein (P-gp)
Breast cancer resistance protein (BCRP)
Drug efflux transporter
GF120918 (elacridar)
XR9576 (tariquidar)

ABSTRACT

The purpose of this study was to synthesize two new positron emission tomography (PET) probes, *N*-(4-(2-(1,2,3,4-tetrahydro-6,7-dimethoxy-2-isoquinolinyl)ethyl)phenyl)-9,10-dihydro-5-[^{18}F]fluoroethoxy-9-oxo-4-acridine carboxamide ([^{18}F]**3**) and quinoline-3-carboxylic acid [2-(4-{2-[7-(2-[^{18}F]fluoroethoxy)-6-methoxy-3,4-dihydro-1*H*-isoquinolin-2-yl]ethyl}phenylcarbamoyl)-4,5-dimethoxyphenyl]amide ([^{18}F]**4**), and to evaluate the potential of these PET probes for assessing the function of two major drug efflux transporters, P-glycoprotein (P-gp) and breast cancer resistance protein (BCRP). [^{18}F]**3** and [^{18}F]**4** were synthesized by ^{18}F-alkylation of each *O*-desmethyl precursor with [^{18}F]2-fluoroethyl bromide for injection as PET probes. In vitro accumulation assay showed that treatment with P-gp/BCRP inhibitors (**1** and **2**) enhanced the intracellular accumulation capacity of P-gp- and BCRP-overexpressing MES-SA/Dx5 cells. In PET studies, the uptake ($AUC_{brain\ [0–60\ min]}$) of [^{18}F]**3** and [^{18}F]**4** in wild-type mice co-injected with **1** were approximately sevenfold higher than that in wild-type mice, and the uptake of [^{18}F]**3** and [^{18}F]**4** in P-gp/Bcrp knockout mice were eight- to ninefold higher than that in wild-type mice. The increased uptake of [^{18}F]**3** and [^{18}F]**4** was similar to that of parent compounds ([^{11}C]**1** and [^{11}C]**2**) previously described, indicating that radioactivity levels in the brain after injection of [^{18}F]**3** and [^{18}F]**4** are related to the function of drug efflux transporters. Also, these results suggest that the structural difference between parent compounds ([^{11}C]**1** and [^{11}C]**2**) and fluoroethyl analogs ([^{18}F]**3** and [^{18}F]**4**) do not obviously affect the potency against drug efflux transporters. In metabolite analysis of mice, the unchanged form in the brain and plasma at 60 min after co-injection of [^{18}F]**4** plus **1** were higher (95% for brain; 81% for plasma) than that after co-injection of [^{18}F]**3** plus **1**. [^{18}F]**4** is a promising PET probe to assess the function of drug efflux transporters.

1. Introduction

Drug efflux transporters have a major impact on the pharmacological behavior of drugs, critically affecting its absorption, disposition, and elimination from organs and tissues.[1–4] These transporters are known to limit absorption across many biological barriers and restrict entry into important pharmacological sites.[3] The most extensively characterized drug efflux transporters are ATP-binding cassette transporters, which include P-glycoprotein (P-gp), multidrug resistance-associated proteins (MRPs), and breast cancer resistance protein (BCRP).[2,5] Furthermore, multidrug resistance (MDR) is primarily caused by cellular extrusion of drugs by drug efflux transporters.

The acridone carboxamide derivative GF120918 (**1**, elacridar, Scheme 1) and anthranilic acid derivative XR9576 (**2**, tariquidar, Scheme 1) were developed as third-generation MDR inhibitors.[6,7] Compound **1** is active against P-gp, which is about 100-fold as potent as cyclosporin A and verapamil.[6] It can also reverse BCRP-mediated drug resistance in human and murine cell lines.[8,9] Compound **2** inhibits the basal ATPase activity associated with P-gp, suggesting that the modulating effect of **2** is derived from the inhibition of substrate binding, ATP hydrolysis, or both.[10] Inhibitory activity of **2** against P-gp function is higher than that of typical P-gp modulators, although **2** slightly inhibits BCRP function.[11]

[^{11}C]**1** and [^{11}C]**2** (Scheme 1) have been developed as positron emission tomography (PET) probes for evaluating drug efflux transporters.[12–15] In PET studies using [^{11}C]**1** and [^{11}C]**2**, the radioactivity level for 60 min after injection in P-gp/Bcrp knockout mice were nine- and 11-fold higher than that in wild-type mice,

* Corresponding author. Tel.: +81 43 206 3192; fax: +81 43 206 3241.
E-mail address: kawamur@nirs.go.jp (K. Kawamura).

0968-0896/$ - see front matter © 2010 Elsevier Ltd. All rights reserved.
doi:10.1016/j.bmc.2010.12.004

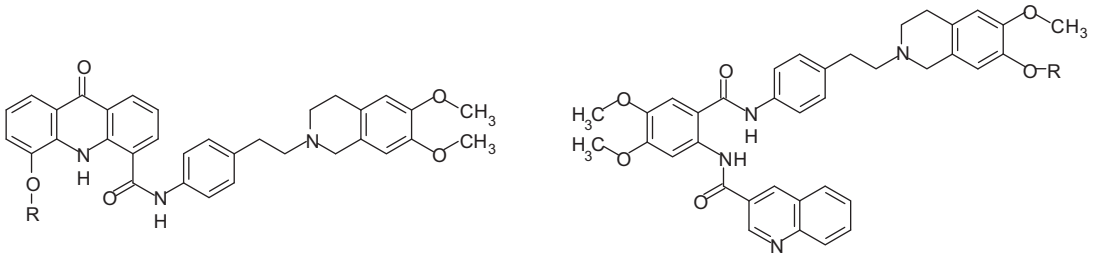

1: R = CH_3
3: R = CH_2CH_2F
[^{11}C]**1**: R = $^{11}CH_3$
[^{18}F]**3**: R = $CH_2CH_2{}^{18}F$

2: R = CH_3
4: R = CH_2CH_2F
[^{11}C]**2**: R = $^{11}CH_3$
[^{18}F]**4**: R = $CH_2CH_2{}^{18}F$

Scheme 1. Chemical structures of GF120918 (**1**), XR9576 (**2**), and fluoroethyl analogs **3** and **4**.

respectively.[13,14] We demonstrated that increased radioactivity levels in P-gp/Bcrp knockout and wild-type mice for 60 min after injection of [^{11}C]**1** and [^{11}C]**2** is correlated with the function of drug efflux transporters. We suggest that [^{11}C]**1** and [^{11}C]**2** are useful PET probes and accumulation of these probes helps assess the function of drug efflux transporters.[13,14]

Here we developed [^{18}F]fluoroethyl analog of **1**, *N*-(4-(2-(1,2,3,4-tetrahydro-6,7-dimethoxy-2-isoquinolinyl)ethyl)phenyl)-9,10-dihydro-5-[^{18}F]fluoroethoxy-9-oxo-4-acridine carboxamide ([^{18}F]**3**, Scheme 1) and [^{18}F]fluoroethyl analog of **2**, quinoline-3-carboxylic acid [2-(4-{2-[7-(2-[^{18}F]fluoroethoxy)-6-methoxy-3,4-dihydro-1*H*-isoquinolin-2-yl]ethyl}phenylcarbamoyl)-4,5-dimethoxyphenyl]amide ([^{18}F]**4**, Scheme 1) to enhance the effectiveness of probes for evaluating the function of drug efflux transporters.

2. Results

2.1. Chemistry

Compounds **3** and **4** were synthesized according to the reaction sequences delineated in Schemes 2 and 3. Alkylation of **5**[13] with 1-iodo-2-fluoroethane in *N,N*-dimethylformamide (DMF) containing potassium carbonate at 80 °C for 2 h gave **3** with a chemical yield of 62%. Compound **4** was synthesized in three-steps as mentioned below. Alkylation of **6**[14] with 1-iodo-2-fluoroethane containing potassium carbonate as a base in DMF at 80 °C for 2 h gave **7**, and reductive amination of **7** gave **8**. Reaction of **8** with quinoline-3-carbonyl chloride in dichloromethane at room temperature for 7 h gave **4** with a chemical yield of 24% from **6**.

2.2. Computation of *c* Log *D*

c Log *D* (at pH 7.4) values for **3** and **4** were 5.62 and 5.12, respectively.

2.3. Radiosynthesis

All synthetic sequences of [^{18}F]**3** and [^{18}F]**4** were carried out using an in-house automated synthesis system.[16] [^{18}F]2-Fluoroethyl bromide was synthesized as the alkylating intermediate by the reaction of cyclotron-produced [^{18}F]fluoride ion (F^-) with 2-trifluoromethanesulfonyloxyethylbromide.[17] [^{18}F]**3** and [^{18}F]**4** were synthesized by heating each *O*-desmethyl precursors (**5** or **9**) with [^{18}F]2-fluoroethyl bromide in anhydrous DMF containing tetrabutylammonium hydroxide as a base at 90–120 °C for 10 min. Radiosynthesis times of [^{18}F]**3** and [^{18}F]**4** were 60–70 min from the end of irradiation. Decay-corrected radiochemical yields from [^{18}F]F^- at the end of synthesis (EOS) were 4.7 ± 1.9% (n = 6) and 1.5 ± 0.9% (n = 6), respectively. The specific activity of [^{18}F]**3** and [^{18}F]**4** was 140–490 TBq/mmol at EOS. Radiochemical yield and specific radioactivity were at levels suitable for injection as PET probes. [^{18}F]**3** and [^{18}F]**4** were identified on analytical high performance liquid chromatography (HPLC) by co-injection with unlabeled **3** and **4**. The radiochemical purity of [^{18}F]**3** and [^{18}F]**4** was >99% and remained equal to 95% after maintaining the formulated product for at least 3 h at room temperature.

2.4. In vitro accumulation assay

Figure 1 shows increased intercellular accumulation of [^{18}F]**3** and [^{18}F]**4** in P-gp- and BCRP-overexpressing MES-SA/Dx5 cells[18–20] treated for 120 min at 37 °C with one of **1**, **2**, **3** and **4** at a concentration of 10 μM compared to untreated cells (control cells). Treatment with all investigated compounds enhanced the tracer accumulation capacity to MES-SA/Dx5 cells. The percentage of increased accumulation of [^{18}F]**3** and [^{18}F]**4** in cells treated with **1** was higher than that treated with other investigated compounds (**2**–**4**). The increased accumulation of [^{18}F]**3** and [^{18}F]**4** in cells treated with **2** was similar to that treated with **3** and **4**.

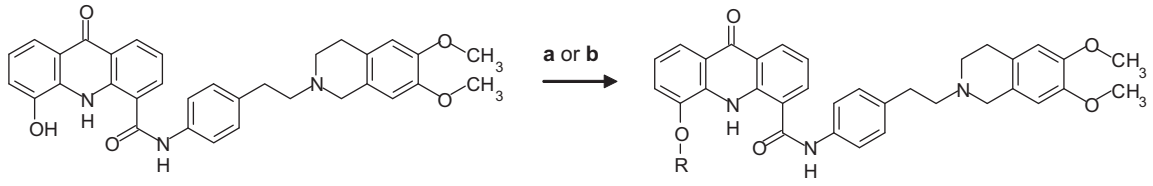

5

3: R = CH_2CH_2F
[^{18}F]**3**: R = $CH_2CH_2{}^{18}F$

Scheme 2. Chemical synthesis of **3** and radiosynthesis of [^{18}F]**3**. Reagents and conditions: (a) 1-iodo-2-fluoroethane, potassium carbonate, *N,N*-dimethylformamide (DMF), 80 °C, 2 h, yield 62%; (b) [^{18}F]2-fluoroethyl bromide, tetrabutylammonium hydroxide, DMF, 80 °C, 10 min, 4.7% radiochemical yield (RCY) from [^{18}F]F^-.

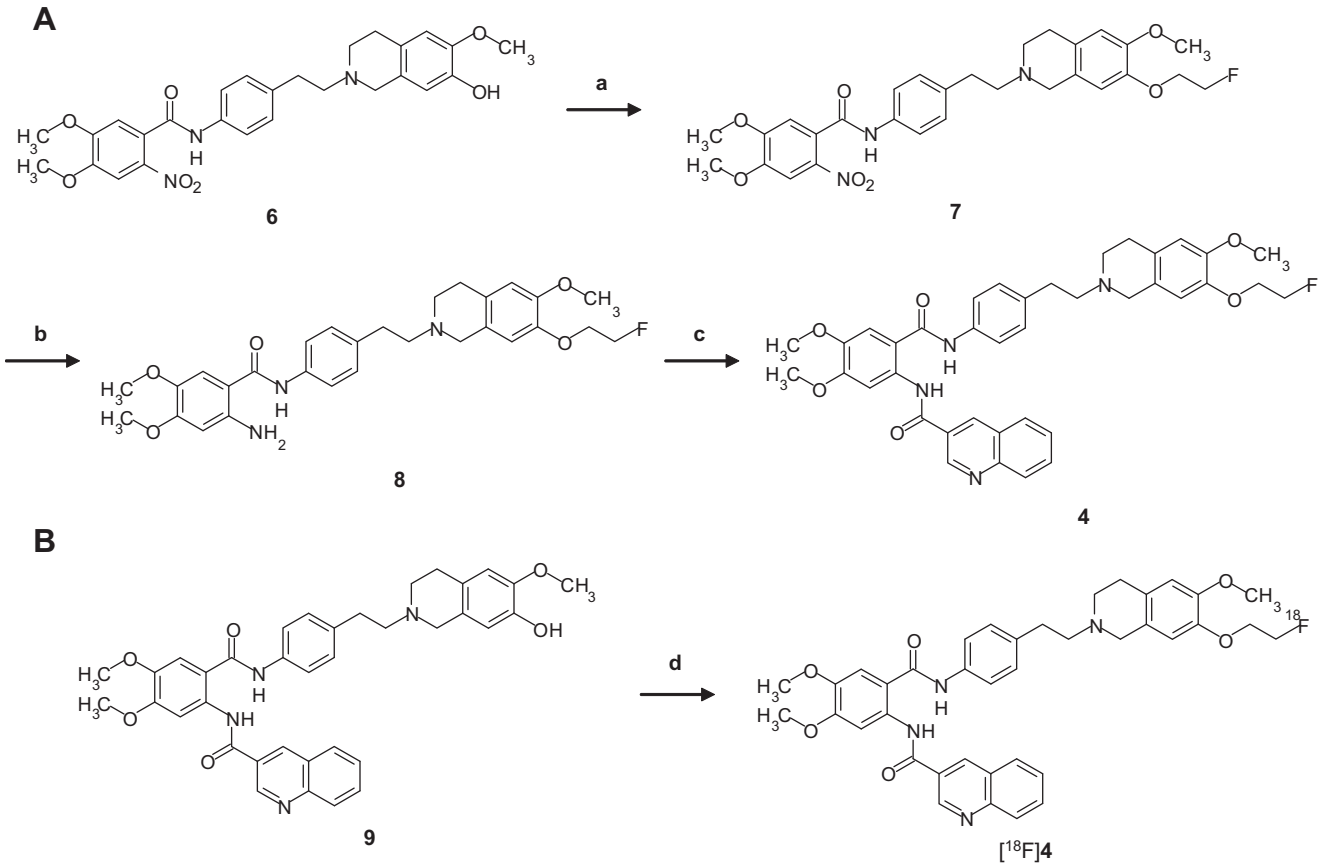

Scheme 3. Chemical synthesis of **4** (A) and radiosynthesis of [^{18}F]**4** (B). Reagents and conditions: (a) 1-iodo-2-fluoroethane, potassium carbonate, DMF, 80 °C, 2 h; (b) ammonium formate, 5% palladium carbon, methanol, reflux, 6 h; (c) quinoline-3-carbonyl chloride, dichloromethane, rt, 7 h, yield 24%; (d) [^{18}F]2-fluoroethyl bromide, tetrabutylammonium hydroxide, DMF, 80 °C, 10 min, 1.5% RCY from [^{18}F]F$^-$.

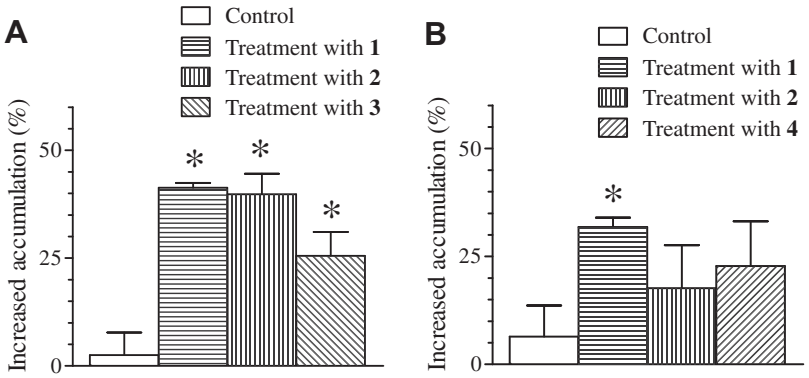

Figure 1. Increased intercellular accumulation of [^{18}F]**3** (A) or [^{18}F]**4** (B) in MES-SA/Dx5 cells treated with **1**, **2**, **3** and **4** (10 μM) for 120 min at 37 °C compared to untreated cells (control cells). Data was triplicate. *Significant difference (P <0.05) compared with the control (one-way ANOVA and Dunnett's post hoc tests). *Abbreviation*: N.D., not determined.

2.5. Biodistribution in mice

Tables 1 and 2 summarize tissue distribution of radioactivity after injection of [^{18}F]**3** and [^{18}F]**4** in mice. As for [^{18}F]**3**, the radioactivity level in the brain was the lowest of all tissues investigated. While radioactivity levels in the pancreas, liver and small intestine gradually increased, levels in the blood, heart, lung, and muscle gradually decreased, and levels in the spleen, kidney, bone, and brain were maintained at a constant level after initial uptake. As for [^{18}F]**4**, the radioactivity level in the brain was also the lowest of all tissues investigated. While levels in the pancreas, spleen, and small intestine gradually increased, and levels in the blood, heart, lung, kidney, and muscle gradually decreased, and levels in the bone and brain were maintained at a constant level after initial uptake. In contrast, the radioactivity level in the liver gradually increased until 15 min after injection of [^{18}F]**4** and was then maintained at a constant level.

To evaluate whether drug efflux transporters mediated penetration of radioactivity in the brain and testis after injection of [^{18}F]**3** or [^{18}F]**4**, we investigated the effects of co-injection with **1** in the brain, testis, and blood after injection of [^{18}F]**3** and [^{18}F]**4** in mice (Fig. 2). Co-injection with **1** (5 mg/kg) induced approximately a

Table 1
Tissue distribution of radioactivity after injection of [^{18}F]**3**

	Radioactivity level[a] (%ID/g)				
	5 min	15 min	30 min	60 min	90 min
Blood	1.39 ± 0.12	0.72 ± 0.09	0.65 ± 0.37	0.40 ± 0.04	0.36 ± 0.04
Heart	6.65 ± 0.55	2.43 ± 0.15	1.38 ± 0.09	1.19 ± 0.06	0.85 ± 0.02
Lung	19.60 ± 0.96	13.32 ± 1.05	7.21 ± 0.50	6.16 ± 1.27	4.09 ± 0.45
Liver	4.88 ± 0.36	5.99 ± 0.73	5.35 ± 0.38	11.60 ± 1.26	14.82 ± 1.04
Pancreas	6.12 ± 1.87	9.68 ± 0.71	11.15 ± 2.52	15.14 ± 1.58	15.21 ± 1.44
Spleen	4.76 ± 0.51	5.34 ± 0.50	5.82 ± 0.34	5.74 ± 0.55	4.71 ± 0.24
Kidney	20.65 ± 1.58	24.17 ± 2.08	19.45 ± 1.05	23.44 ± 2.44	19.98 ± 1.32
Small intestine	4.51 ± 0.39	7.09 ± 0.57	7.60 ± 1.29	12.48 ± 1.07	17.15 ± 2.25
Muscle	1.75 ± 0.14	1.18 ± 0.18	0.62 ± 0.03	0.53 ± 0.04	0.38 ± 0.05
Bone	1.99 ± 0.27	1.66 ± 0.21	1.63 ± 0.22	1.43 ± 0.38	1.30 ± 0.22
Brain	0.18 ± 0.00	0.16 ± 0.01	0.14 ± 0.01	0.17 ± 0.02	0.13 ± 0.02

[a] Mean ± SD (n = 4); percentage of injected dose/gram tissue (%ID/g).

Table 2
Tissue distribution of radioactivity after injection of [^{18}F]**4**

	Radioactivity level[a] (%ID/g)				
	5 min	15 min	30 min	60 min	90 min
Blood	1.39 ± 0.09	0.88 ± 0.05	0.63 ± 0.04	0.61 ± 0.02	0.57 ± 0.02
Heart	7.44 ± 0.85	3.49 ± 0.31	2.86 ± 0.24	2.09 ± 0.13	1.74 ± 0.17
Lung	22.50 ± 2.58	20.55 ± 1.94	17.89 ± 1.29	16.06 ± 1.53	15.76 ± 2.05
Liver	29.33 ± 2.30	31.06 ± 0.63	23.23 ± 3.31	25.40 ± 2.82	22.18 ± 2.26
Pancreas	6.05 ± 0.60	8.27 ± 0.84	8.56 ± 0.35	12.45 ± 0.68	13.56 ± 1.09
Spleen	5.12 ± 0.67	6.73 ± 0.10	6.34 ± 0.40	7.18 ± 0.27	7.42 ± 0.94
Kidney	18.00 ± 1.79	16.09 ± 0.98	11.34 ± 1.17	11.29 ± 0.52	10.17 ± 0.73
Small intestine	5.67 ± 0.67	9.42 ± 1.42	14.09 ± 1.61	22.42 ± 1.57	24.45 ± 2.38
Muscle	2.23 ± 0.24	1.61 ± 0.18	1.04 ± 0.12	0.92 ± 0.13	0.68 ± 0.06
Bone	2.17 ± 0.20	1.85 ± 0.23	1.45 ± 0.32	1.62 ± 0.20	1.45 ± 0.12
Brain	0.13 ± 0.02	0.11 ± 0.01	0.11 ± 0.00	0.10 ± 0.00	0.10 ± 0.01

[a] Mean ± SD (n = 4); percentage of injected dose/gram tissue (%ID/g).

10- and seven-fold increase in the brain-to-blood and testis-to-blood ratios of radioactivity after injection of [^{18}F]**3**, respectively. Similarly, co-injection with **1** induced a 10- and fivefold increase in the brain-to-blood and testis-to-blood ratios of radioactivity after injection of [^{18}F]**4**, respectively.

2.6. Metabolite analysis in the brain and plasma of mice co-injected with 1

To evaluate the role played by radiolabeled metabolites in increased accumulation after co-injection of [^{18}F]**3** or [^{18}F]**4** by inhibiting drug efflux transporters, we investigated the percentages of unchanged forms in the brain and plasma at 30 and 60 min after co-injection of [^{18}F]**3** plus **1** (5 mg/kg) or [^{18}F]**4** plus **1** (5 mg/kg) (Table 3). The percentage of unchanged form in the brain and plasma at 30 min after co-injection of [^{18}F]**3** plus **1** was higher than that at 60 min after co-injection. In contrast, a significant difference was not observed in the percentage form in the brain and plasma at 30 and 60 min after co-injection of [^{18}F]**4** plus **1**. In the plasma, the percentage of unchanged form after co-injection of [^{18}F]**4** plus **1** was higher than that after co-injection of [^{18}F]**3** plus **1** at both 30 and 60 min. In the brain, the percentage of unchanged form at 60 min after co-injection of [^{18}F]**4** plus **1** was higher than that after co-injection of [^{18}F]**3** plus **1**.

Radiolabeled metabolites with high polarity were observed on each HPLC chart. The eluting time from the column of metabolite for [^{18}F]**3** and [^{18}F]**4** were 1.8 and 1.9 min, respectively. After injection of [^{18}F]**3**, recovery of radioactivity from brain tissue and

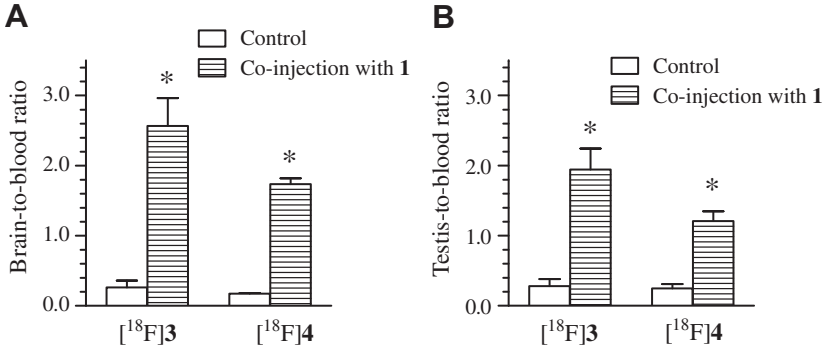

Figure 2. Effects of co-injection with **1** on the brain-to-blood (A) and testis-to-blood (B) ratios at 30 min after injection of [^{18}F]**3** and [^{18}F]**4** into mice (n = 4 per group). Injected dose of ^{18}F -labeled ligands was 1.0–4.8 MBq. Co-injected dose of **1** was 5 mg/kg. *Significant difference (P <0.05) compared with the control (one-way ANOVA and Dunnett's post hoc tests).

plasma into acetonitrile for deproteinized treatment were 91.4 ± 5.3% (n = 7) and 94.1 ± 1.2% (n = 7), respectively. After injection of [^{18}F]**4**, recovery of radioactivity from brain tissue and plasma into acetonitrile for deproteinized treatment were 92.5 ± 1.6% (n = 7) and 95.3 ± 1.3% (n = 7), respectively. Recovery of radioactivity from HPLC analysis was essentially quantitative.

2.7. PET studies in wild-type and P-gp/Bcrp knockout mice

To evaluate whether brain penetration of [^{18}F]**3** and [^{18}F]**4** is related to the function of drug efflux transporters, we further performed PET studies using [^{18}F]**3** and [^{18}F]**4** in wild-type mice co-injected with or without **1** and in P-gp and/or Bcrp knockout mice (Figs. 3 and 4). In wild-type mice, the radioactivity level in the brain after injection of [^{18}F]**3** or [^{18}F]**4** was low (Fig. 3). Co-injection with **1** induced an increase in the radioactivity level of the brain after injection of [^{18}F]**3** or [^{18}F]**4** (Fig. 3). In P-gp/Bcrp knockout mice, the radioactivity level in the brain after the injection of [^{18}F]**3** and [^{18}F]**4** was distributed throughout the brain (Fig. 3). In P-gp/Bcrp knockout mice, the radioactivity level in the brain after injection of [^{18}F]**3** was maintained at a constant level after initial uptake for 60 min after injection (Fig. 4A). After injection of [^{18}F]**4**, radioactivity levels in the brain increased gradually after initial uptake (Fig. 4B). In P-gp knockout mice, the radioactivity level in the brain after injection of [^{18}F]**3** and [^{18}F]**4** was gradually decreased after initial uptake, and that was maintained at higher level than that in wild-type mice for 60 min after injection (Fig. 4). In Bcrp knockout mice, the radioactivity level in the brain after injection of [^{18}F]**3** and [^{18}F]**4** was gradually decreased after initial uptake, and that was almost identical to that of wild-type mice (Fig. 4). In wild-type mice co-injected with **1**, the radioactivity level in the brain after injection of [^{18}F]**3** decreased gradually after initial uptake for 60 min after injection (Fig. 4A). After injection of [^{18}F]**4**, radioactivity level in the brain increased gradually after initial uptake and maintained constant level for over 30 min after injection (Fig. 4B). In the blood, the time–activity curve (TAC) in wild-type mice after injection of [^{18}F]**3** and [^{18}F]**4** were similar pattern to that in P-gp and/or Bcrp knockout mice (Fig. 5).

The area under the time-activity curve (AUC) of the region of interest (ROI) in the brain from 0 to 60 min ($AUC_{brain\ [0–60\ min]}$) after injection of [^{18}F]**3** in P-gp/Bcrp knockout mice was 9.0-fold higher than that in wild-type mice (39.8 ± 1.8 for P-gp/Bcrp knockout mice; 4.4 ± 0.5 for wild-type mice; n = 4 each group), and that in P-gp knockout mice after injection of [^{18}F]**3** was 2.4-fold higher than that in wild-type mice (10.6 ± 0.6 for P-gp knockout mice, n = 4). However, $AUC_{brain\ [0–60\ min]}$ in Bcrp knockout mice after injection of [^{18}F]**3** was almost identical to that of wild-type mice (5.0 ± 0.7 for Bcrp knockout mice, n = 4). Also, $AUC_{brain\ [0–60\ min]}$ in wild-type mice after co-injection of [^{18}F]**3** plus **1** was 6.9-fold higher than that in wild-type mice (30.2 ± 2.0 for wild-type mice co-injected with **1**, n = 4). In addition, $AUC_{brain\ [0–60\ min]}$ after injection of [^{18}F]**4** in P-gp/Bcrp knockout mice was 8.3-fold higher than that in wild-type mice (32.9 ± 2.5 for P-gp/Bcrp knockout mice; 4.0 ± 0.2 for wild-type mice; n = 4 each group), and that in P-gp knockout mice after injection of [^{18}F]**4** was 2.3-fold higher than that in wild-type mice (9.1 ± 1.8 for P-gp knockout mice, n = 4). However, $AUC_{brain\ [0–60\ min]}$ in Bcrp knockout mice after injection of [^{18}F]**4** was almost identical to that of wild-type mice (6.5 ± 0.8 for Bcrp knockout mice, n = 4). Also, $AUC_{brain\ [0–60\ min]}$ in wild-type mice after co-injection of [^{18}F]**4** plus **1** was 7.1-fold higher than that in wild-type mice (28.1 ± 3.3 for wild-type mice co-injected with **1**, n = 4). No significant differences were observed in the AUC of ROI in the blood from 0 to 60 min ($AUC_{blood\ [0–60\ min]}$) after injection of [^{18}F]**3** among wild-type (25.6 ± 5.3), P-gp/Bcrp knockout (25.0 ± 3.6), P-gp knockout (23.5 ± 4.6) and Bcrp knockout mice (25.3 ± 6.9). Also, there are no significant differences in $AUC_{blood\ [0–60\ min]}$ after injection of [^{18}F]**4** among wild-type (33.2 ± 5.7), P-gp/Bcrp knockout (33.9 ± 5.0), P-gp knockout (45.0 ± 8.1) and Bcrp knockout mice (42.2 ± 11.6).

Table 3
Metabolite analysis in the brain and plasma of mice at 30 and 60 min after co-injection of [^{18}F]**3** plus **1** (5 mg/kg) and [^{18}F]**4** plus **1** (5 mg/kg)

	Unchanged form[a] (%)			
	Brain		Plasma	
	30 min	60 min	30 min	60 min
[^{18}F]**3** plus **1** (5 mg/kg)	95.9 ± 0.8	88.2 ± 2.7*	69.6 ± 1.5	48.8 ± 4.5*
[^{18}F]**4** plus **1** (5 mg/kg)	95.7 ± 0.3	95.4 ± 2.9**	89.3 ± 1.2**	80.8 ± 5.8**

[a] Mean ± SD (n = 3–4).
* Significant difference (P <0.05) in the percentages of unchanged form in the brain and plasma at 30 and 60 min after injection.
** Significant difference (P <0.05) between co-injections of [^{18}F]**3** plus **1** and [^{18}F]**4** plus **1**.

3. Discussion

Compound **3** was synthesized by alkylation of its *O*-desmethyl precursor **5** with 1-iodo-2-fluoroethane and commercially available materials. We attempted direct alkylation of **9** with 1-iodofluoroethane or 1-bromofluoroethane in the presence of a base, but the reaction did not proceed efficiently because of hydrolysis of the amide between quinoline and dimethoxybenzene. We determined another three-step route to accomplish the synthesis of **4**. Fluoroethylation of **6** followed by reduction of the nitro group gave **8**, which was acylated with quiniline-3-carbonyl chloride to produce **4**.

[^{18}F]**3** and [^{18}F]**4** were readily synthesized by alkylation of each *O*-desmethyl precursor (**5** or **9**) with [^{18}F]2-fluoroethyl bromide, which was synthesized from the cyclotron-produced [^{18}F]F^- and 2-trifluoromethanesulfonyloxyethylbromide. Purification by HPLC gave [^{18}F]**3** and [^{18}F]**4** with radiochemical yields, radiochemical purity, and specific radioactivity suitable for injection as PET probes. Formulated PET probes were radiochemically stable.

Previously, de Vries et al. and we suggested that P-gp and Bcrp act in concert to limit brain penetration of drugs,[21] such as [^{11}C]**1** and [^{11}C]**2**.[13,14] In addition, Kannan et al. suggested that some inhibitors of ABC transporters may lose selectivity for one ABC transporter at high concentrations.[22] For example, low concentrations (⩽100 nM) of tariquidar appear to be selective for P-gp, but higher concentrations (>1 μM) show cross reactivity for BCRP. Therefore, we considered that it is important to assess affinity for both P-gp and BCRP to evaluate the function of drug efflux transporters.[22] Parent compound **1** is a dual P-gp and BCRP inhibitor, and parent compound **2** is a P-gp inhibitor. However, recent in vivo studies suggest that tracer amounts (injected dose, >0.5 nmol) of [^{11}C]**1**, [^{11}C]**2**, [^{11}C]*N*-desmethylloperamide and [^{11}C]laniquidar (MDR inhibitor) act as a substrate for drug efflux transporters.[13,14,22,23] Tracer amounts of [^{18}F]**3** and [^{18}F]**4** are also predicted to act as a substrate for drug efflux transporters. Furthermore, compounds **3** and **4** may display similar in vitro and in vivo property to compounds **1** and **2**, because of the molecular similarity and bioisosteric property of *O*-CH_3CH_2F with *O*-CH_3 group. Therefore, we evaluated the usefulness of [^{18}F]**3** and [^{18}F]**4** as PET probes to assess the function of drug efflux transporters by in vivo studies.

In the in vitro accumulation assay, treatment of P-gp- and BCRP-overexpressing MES-SA/Dx5 cells[18–20] with **1** resulted in a remarkable increase in the accumulation of [^{18}F]**3** and [^{18}F]**4** (Fig. 1), indicating active transport and efflux of [^{18}F]**3** and [^{18}F]**4** by MES-SA/Dx5 cells. On the other hand, the increased accumulation of [^{18}F]**3** in cells treated with **3** (26%) was lower than that of [^{18}F]**3** treated with **1** (41%) (Fig. 1). Also, the increased

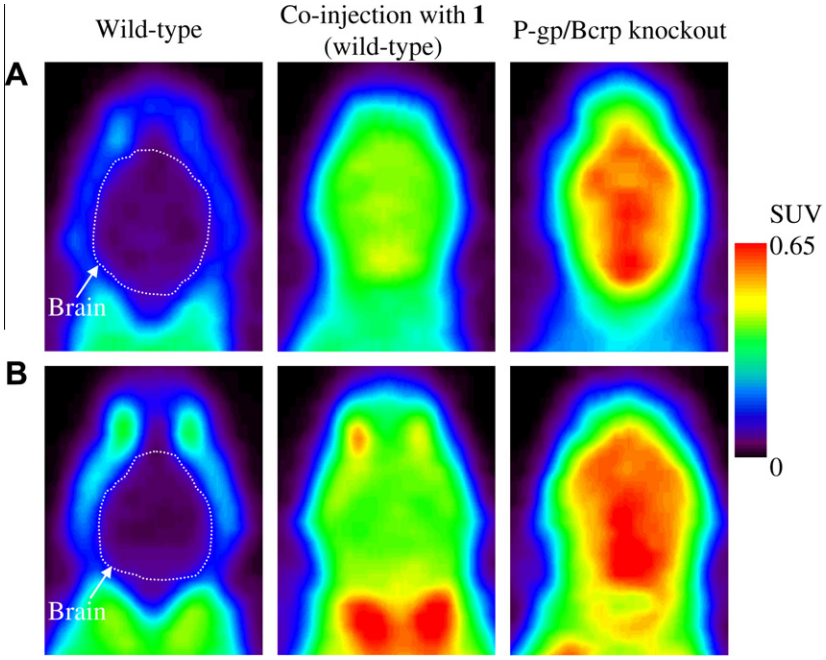

Figure 3. Typical coronal PET images showing [^{18}F]**3** (A) and [^{18}F]**4** (B) in the brain of wild-type mouse, wild-type mouse co-injected with **1**, and a P-gp/Bcrp knockout mouse. The injected dose of [^{18}F]**3** and [^{18}F]**4** was 3.3–4.9 MBq. Co-injected dose of **1** was 5.0 mg/kg. PET images were obtained from 0 to 60 min after injection. Mice were anesthetized with isoflurane and fixed in a prone position on the bed of the scanner. The radioactivity level was expressed as the standardized uptake value (SUV).

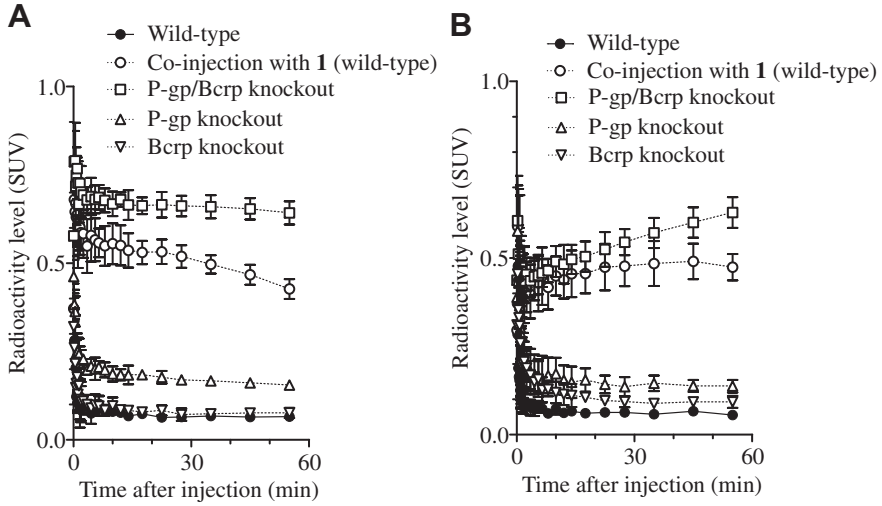

Figure 4. Time–activity curves of the brain after injection of [^{18}F]**3** (A) and [^{18}F]**4** (B) in wild-type mice, wild-type mice co-injected with **1**, P-gp/Bcrp knockout mice, P-gp knockout mice and Bcrp knockout mice (n = 4–6 per group). The injected dose of [^{18}F]**3** and [^{18}F]**4** was 2.8–5.6 MBq. The radioactivity level was expressed as SUV.

accumulation of [^{18}F]**4** in cells treated with **4** (23%) was lower than that of [^{18}F]**4** treated with **1** (32%) (Fig. 1). These results suggest that the inhibitory effect on the function of drug efflux transporter by treatment with **3** or **4** is weaker than that by the parent compound **1**. Based on these in vitro results, it is suggested that [^{18}F]**3** and [^{18}F]**4** are modulated by the function of drug efflux transporters as substrates.

In in vivo tissue distribution, the radioactivity level in the brain at 30 min after injection of [^{18}F]**3** and [^{18}F]**4** was the lowest of all tissues investigated (Tables 1 and 2), due to relatively high lipophilicity (*c* Log *D*, 5.6 for **3**; 5.1 for **4**). Co-injection with **1** (5 mg/kg) induced a significant increase in the brain uptake at 30 min after injection of [^{18}F]**3** and [^{18}F]**4** (Fig. 3). Furthermore, $AUC_{brain\ [0–60\ min]}$ after injection of [^{18}F]**3** and [^{18}F]**4** in wild-type mice co-injected with **1** were approximately sevenfold higher than that in wild-type mice, and $AUC_{brain\ [0–60\ min]}$ in P-gp/Bcrp knockout mice were eight- to ninefold higher than that in wild-type mice (Fig. 4). Previously, we evaluated [^{11}C]**1** and [^{11}C]**2** as PET probes to assess the function of drug efflux transporters using small-animal PET measurements.[13,14] $AUC_{brain\ [0–60\ min]}$ in P-gp/Bcrp knockout mice after injection of [^{11}C]**1** and [^{11}C]**2** were approximately nine- and 11-fold higher than that in wild-type mice, respectively.[13,14] The increased uptake after injection of [^{18}F]**3** and [^{18}F]**4** was similar to that of [^{11}C]**1** and [^{11}C]**2**. As previously described for [^{11}C]**1** and [^{11}C]**2**, these results indicate that radioactivity levels in the brain after injection of [^{18}F]**3** and [^{18}F]**4** are related to the function of drug efflux transporters. Also, these results suggest that the structural difference between parent

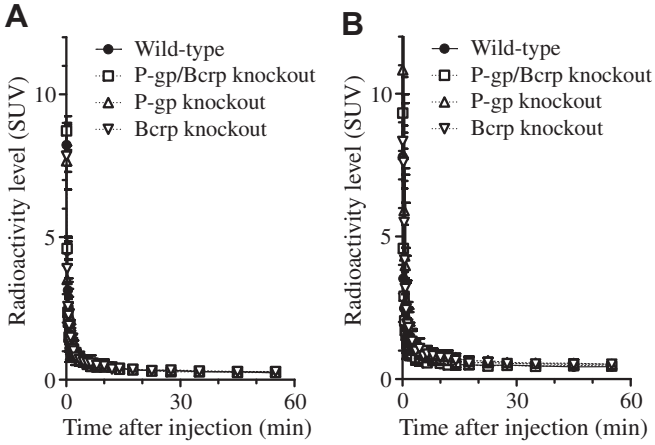

Figure 5. Time–activity curves of the blood after injection of [^{18}F]**3** (A) and [^{18}F]**4** (B) in wild-type mice, P-gp/Bcrp knockout mice, P-gp knockout mice and Bcrp knockout mice (n = 4–6 per group). The injected dose of [^{18}F]**3** and [^{18}F]**4** was 2.8–5.6 MBq. The radioactivity level was expressed as SUV.

compounds ([^{11}C]**1** and [^{11}C]**2**) and fluoroethyl analogs ([^{18}F]**3** and [^{18}F]**4**) do not obviously affect the potency against drug efflux transporters. In the metabolite study using mice co-injected with **1**, [^{18}F]**3** and [^{18}F]**4** showed a high metabolic stability at 30 and 60 min after injection in the brain (Table 3), indicating that the radioactive metabolites scarcely affect the uptake of [^{18}F]**3** and [^{18}F]**4** in the brain. These results suggest that excretion of [^{18}F]**3** or [^{18}F]**4** itself from the brain is related to drug efflux transporters. Therefore, radio-metabolites after injection of [^{18}F]**3** or [^{18}F]**4** in the plasma are considered to have an little effect on the radioactivity level in the brain, although the percentage of unchanged [^{18}F]**3** (70%) and [^{18}F]**4** (89%) in plasma were lower than that of [^{11}C]**1** (96%)[13] or [^{11}C]**2** (93%)[14] at 30 min after injection. In general, the short half-life of the ^{11}C-labeled probe often limits its usefulness if a dynamic PET experiment has a turnover time longer than 100 min. Since ^{18}F has the advantages of a longer half-life (110 min vs 20 min) and lower positron energy (650 keV vs 960 keV) compared to ^{11}C, the ^{18}F-labeled probe produce high quality images with a high spatial resolution in PET measurements. Moreover, long-distance transportation of ^{18}F to other facilities can be conveniently performed. Therefore, [^{18}F]**3** and [^{18}F]**4** are more useful PET probes than [^{11}C]**1** and [^{11}C]**2** to assess the function of drug efflux transporters.

In PET studies, the $AUC_{brain\ [0–60\ min]}$ after injection of [^{18}F]**3** and [^{18}F]**4** in P-gp knockout mice were approximately 3.6- to 3.8-fold lower than that in P-gp/Bcrp knockout mice, although the $AUC_{brain\ [0–60\ min]}$ value in P-gp knockout mice was approximately 2.3- to 2.4- fold higher than that in wild-type mice (Fig. 4). As previously described for [^{11}C]**1** and [^{11}C]**2**, the expression of Bcrp in P-gp knockout mouse might be sufficient to limit brain penetration of [^{18}F]**3** and [^{18}F]**4**, because the mRNA levels of Bcrp in P-gp knockout mice were three times higher than that in wild-type mice.[24] Additionally, it has been suggested that P-gp and Bcrp functions in the brain concertedly limit brain penetration of shared substrates.[21,25] Therefore, it is considered that P-gp and Bcrp act in concert to limit brain penetration of [^{18}F]**3** and [^{18}F]**4**.

Defluorination is a major issue for some ^{18}F-labeled probes. The [^{18}F]F^- formed by defluorination of ^{18}F-labeled probes binds avidly to the bone, including the skull.[26] Considering biodistribution in mice, radioactivity levels in the bone at 60 min after injection of [^{18}F]**3** and [^{18}F]**4** were relatively low ([^{18}F]**3**, 0.40 standardized uptake value (SUV); [^{18}F]**4**, 0.42 SUV) (Table 1 and 2). These radioactivity levels in the bone were same as that at 60 min after injection of [^{11}C]**1** and [^{11}C]**2** (0.55 SUV and 0.45 SUV).[13,14] These results suggest that defluorination of [^{18}F]**3** and [^{18}F]**4** does not occur in mice.

In PET studies, the radioactivity level in the brain of P-gp/Bcrp knockout mice after injection of [^{18}F]**3** was maintained at a constant level after initial uptake for 60 min after injection, and that in the brain of wild-type mice co-injected with **1** decreased gradually after initial uptake for 60 min after injection (Fig. 3). On the other hand, the radioactivity level in the brain after injection of [^{18}F]**4** had a tendency to accumulate after initial uptake (Fig. 4). This variation in kinetics of the brain between [^{18}F]**3** and [^{18}F]**4** can be explained by radiolabeled metabolites in the brain and plasma. In the metabolite study, the percentage of unchanged form in the brain at 60 min after co-injection of [^{18}F]**4** plus **1** (95%) was higher than that of [^{18}F]**3** plus **1** (88%) (Table 3). In addition, the percentage of unchanged form in the plasma at 30 and 60 min after co-injection of [^{18}F]**4** plus **1** (89% for 30 min, 81% for 60 min) was higher than that of [^{18}F]**4** plus **1** (70% for 30 min, 49% for 60 min) (Table 3). [^{18}F]**4** exhibits a higher metabolic stability than [^{18}F]**3**. Therefore, [^{18}F]**4** may be more suitable than [^{18}F]**3** to evaluate in vivo the function of drug efflux transporters.

4. Conclusions

We synthesized and evaluated new PET probes, [^{18}F]**3** and [^{18}F]**4**, to assess the function of drug efflux transporters. [^{18}F]**3** and [^{18}F]**4** were synthesized by ^{18}F-alkylation of each *O*-desmethyl precursors (**5** and **9**) with [^{18}F]2-fluoroethyl bromide for injection as PET probes. Radioactivity levels after injection of [^{18}F]**3** and [^{18}F]**4** in mice brain increased by inhibiting the function of drug efflux transporters. The increased uptake after injection of [^{18}F]**3** and [^{18}F]**4** was similar to that of [^{11}C]**1** and [^{11}C]**2**. In metabolite analysis of mice brain and plasma, [^{18}F]**4** was more metabolically stable than [^{18}F]**3**. [^{18}F]**4** may be more suitable than [^{18}F]**3** to evaluate in vivo the function of drug efflux transporters. Consequently, [^{18}F]**4** is a promising PET probe to assess the function of drug efflux transporters.

5. Materials and methods

5.1. General

Melting points were uncorrected. Proton nuclear magnetic resonance (^{1}H NMR) and carbon-13 nuclear magnetic resonance (^{13}C NMR) spectra were recorded on the JNM-AL300 spectrometer (Jeol, Tokyo, Japan) using tetramethylsilane as an internal standard. All chemical shifts (δ) were reported in parts per million (ppm) downfield from the standard. High resolution fast atom bombardment-mass spectrometry (FAB-MS) was obtained on a JEOL NMS-SX102 spectrometer (Jeol). Column chromatography was performed using Kieselgel Gel 60 F_{254} (70–230 mesh; Merck, Darmstadt, Germany) or Wakogel C-200 (100–200 mesh; Wako Pure Chemical Industries, Osaka, Japan). HPLC was performed using a Jasco HPLC system (Jasco, Tokyo, Japan). Effluent radioactivity was monitored using a NaI (Tl) scintillation detector system. Compounds **1** and **2** were synthesized in our laboratory as described previously with some modifications.[27,28,7] Reagents and organic solvents were commercially available and used without further purification. If not otherwise stated, radioactivity was determined using an IGC-3R Curiemeter (Aloka, Tokyo, Japan).

5.2. Chemistry

5.2.1. *N*-(4-(2-(1,2,3,4-Tetrahydro-6,7-dimethoxy-2-isoquinolinyl)ethyl)phenyl)-9,10-dihydro-5-fluoroethoxy-9-oxo-4-acridine carboxamide (3)

A mixture of *N*-(4-(2-(1,2,3,4-tetrahydro-6,7-dimethoxy-2-isoquinolinyl)ethyl)phenyl)-9,10-dihydro-5-hydroxy-9-oxo-4-acri-

dine carboxamide[13] (**5**, 52.0 mg, 0.095 mmol), 1-iodo-2-fluoroethane (24.7 mg, 0.142 mmol), potassium carbonate (19.6 mg, 0.142 mmol) in DMF (3 mL) was heated at 80 °C for 2 h. The reaction was quenched with water (5 mL) and extracted with ethyl acetate (5 mL, three times). The organic layer was washed with water and brine, dried over magnesium sulfate, and evaporated in vacuo. The residue was recrystallized from the mixture of chloroform and *n*-hexane, yielding *N*-(4-(2-(1,2,3,4-tetrahydro-6,7-dimethoxy-2-isoquinolinyl)ethyl)phenyl)-9,10-dihydro-5-fluoroethoxy-9-oxo-4-acridine carboxamide (**3**, 35.0 mg, 62%) as a yellow solid. Melting point: 211–212 °C. ^{1}H NMR (300 MHz, $CDCl_3$): δ (ppm) 2.77–2.87 (m, 6H), 2.92–2.97 (m, 2H), 3.67 (s, 2H), 3.85 (s, 6H), 4.44 (t, J = 4.0 Hz, 1H), 4.53 (t, J = 4.0 Hz, 1H), 4.87 (t, J = 4.0 Hz), 5.02 (t, J = 4.0 Hz, 1H), 6.56 (s, 1H), 6.61 (s, 1H), 7.16-7.24 (m, 2H), 7.32 (d, J = 8.4 Hz, 2H), 7.64 (d, J = 8.4 Hz, 2H), 8.01 (dd, J = 1.5, 7.7 Hz, 1H), 8.06 (dd, J = 2.2, 7.3 Hz, 1H), 8.11 (brs, 1H), 8.65 (dd, J = 1.0, 7.7 Hz,1H), 12.24 (s, 1H). ^{13}C NMR (75 MHz, $CDCl_3$): δ (ppm) 28.67, 33.49, 51.03, 55.72, 56.00, 56.05, 59.97, 68.61 (d, J_{C-F} = 21.7 Hz), 81.84 (d, J_{C-F} = 170.8 Hz), 109.87, 111.74, 113.90, 118.93, 119.21, 119.74, 121.02, 121.26, 122.07, 122.66, 126.31, 126.64, 129.37, 131.51, 131.85, 132.14, 135.70, 137.35, 140.22, 146.88, 147.47, 147.79, 166.44, 177.80. High-resolution MS(FAB), *m/z*: 596.2522 (calcd for $C_{35}H_{35}FN_3O_5$: 596.2561). Chemical purity: 98.2% (see Supplementary data).

5.2.2. Quinoline-3-carboxylic acid [2-(4-{2-[7-(2-fluoroethoxy)-6-methoxy-3,4-dihydro-1*H*-isoquinolin-2-yl]ethyl}phenylcarbamoyl)-4,5-dimethoxyphenyl]amide (4)

A mixture of *N*-{4-[2-(7-hydroxy-6-methoxy-3,4-dihydro-1*H*-isoquinolin-2-yl)-ethyl]-phenyl}-4,5-dimethoxy-2-nitrobenzamide[14] (**6**, 82 mg, 0.16 mmol), 1-iodo-2-fluoroethane (62 mg, 0.36 mmol), and potassium carbonate (33 mg, 0.24 mmol) in DMF (5 mL) was heated at 80 °C for 2 h. The reaction mixture was quenched with water (5 mL), and extracted with ethyl acetate (5 mL, two times). The organic layer was washed with water (3 mL) and brine (3 mL), dried over magnesium sulfate, and evaporated in vacuo. The residue was purified by column chromatography on silica gel using a mixture of chloroform and methanol (100:1, v/v) as the mobile phase, yielding *N*-(4-{2-[7-(2-fluoroethoxy)-6-methoxy-3,4-dihydro-1*H*-isoquinolin-2-yl]ethyl}phenyl)-4,5-dimethoxy-2-nitrobenzamide (**7**, 42 mg) as a yellow solid.

Ammonium formate (100 mg) and 5% palladium carbon (20 mg) were added to a solution of **7** (100 mg, 0.18 mmol) in methanol (5 mL). The mixture was refluxed for 6 h. The reaction mixture was filtered through Celite, and evaporated in vacuo. The residue was diluted with chloroform (5 mL), washed with 5% aqueous ammonia (2 mL) and water, and dried over magnesium sulfate. The extract was evaporated in vacuo, yielding 2-amino-*N*-(4-{2-[7-(2-fluoroethoxy)-6-methoxy-3,4-dihydro-1*H*-isoquinolin-2-yl]ethyl}-phenyl)-4,5-dimethoxybenzamide (**8**, 80 mg) as a pale yellow solid.

Quinoline-3-carbonyl chloride (82.1 mg, 0.43 mmol) in dichloromethane (1 mL) was added to a slurry of **8** (160 mg, 0.31 mmol) in dichloromethane (10 mL) and cooled with an ice-water bath. The resulting solution was cooled to room temperature, and stirred for 7 h. The reaction mixture was diluted with dichloromethane, washed with 1 M sodium carbonate and water, dried over magnesium sulfate, and evaporated in vacuo. The residue was purified by column chromatography on silica gel using a mixture of chloroform and methanol (50:1, v/v), yielding quinoline-3-carboxylic acid [2-(4-{2-[7-(2-fluoroethoxy)-6-methoxy-3,4-dihydro-1*H*-isoquinolin-2-yl]ethyl}phenylcarbamoyl)-4,5-dimethoxyphenyl]amide (**4**, 124 mg, 23.7% from **6**) as a pale yellow solid. Melting point: 128–129 °C. ^{1}H NMR (300 MHz, $CDCl_3$): δ (ppm) 2.74–2.94 (m, 8H), 3.63 (s, 2H), 3.73 (s, 3H), 3.82 (s, 3H), 3.90 (s, 3H), 4.17 (t, J = 4.4 Hz, 1H), 4.26 (t, J = 4.4 Hz, 1H), 4.66 (t, J = 4.4 Hz, 1H), 4.82 (t, J = 4.4 Hz, 1H), 6.60 (s, 1H), 6.62 (s, 1H), 7.11 (s, 1H), 7.27 (d, J = 8.4 Hz, 2H), 7.60–7.65 (m, 1H), 7.61 (d, J = 8.4 Hz, 2H), 7.82 (t, J = 7.7 Hz, 1H), 7.98 (d, J = 7.7 Hz, 1H), 8.16 (d, J = 7.7 Hz, 1H), 8.45 (br s, 1H), 8.52 (s, 1H), 8.73 (d, J = 2.0 Hz, 1H), 9.52 (d, J = 2.0 Hz, 1H), 12.44 (br s, 1H). ^{13}C NMR (75 MHz, $CDCl_3$): δ (ppm) 28.73, 33.42, 50.92, 55.55, 55.95, 56.03, 56.23, 60.06, 68.74 (d, J_{C-F} = 21.1 Hz), 81.97 (d, J_{C-F} = 170.2 Hz), 104.86, 109.81, 112.13, 112.27, 112.99, 121.17, 122.74, 126.63, 126.85, 127.14, 127.43, 127.66, 129.16, 129.28, 129.32, 131.42, 135.51, 135.73, 137.24, 144.50, 145.96, 148.36, 148.73, 149.30, 152.61, 163.84, 167.47. High-resolution MS(FAB), *m/z*: 679.2888 (calcd for $C_{39}H_{40}FN_4O_6$: 679.2932). Chemical purity: 95.7% (see Supplementary data).

5.3. Computation of *c* Log *D*

c Log *D* (at pH 7.4) for **3** and **4** were computed using the program Pallas 3.4 (CompuDrug, Sedona, AZ, USA).

5.4. Radiosynthesis of *N*-(4-(2-(1,2,3,4-tetrahydro-6,7-dimethoxy-2-isoquinolinyl)ethyl)phenyl)-9,10-dihydro-5-[^{18}F]fluoroethoxy-9-oxo-4-acridine carboxamide ([^{18}F]3) and quinoline-3-carboxylic acid [2-(4-{2-[7-(2-[^{18}F]fluoroethoxy)-6-methoxy-3,4-dihydro-1*H*-isoquinolin-2-yl]ethyl}phenylcarbamoyl)-4,5-dimethoxyphenyl]amide ([^{18}F]4)

The [^{18}F]F$^-$ was produced from the cyclotron (CYPRIS HM-18; Sumitomo Heavy Industries, Tokyo, Japan) by the ^{18}O (p, n) ^{18}F reaction on 95 atom % $H_2{}^{18}O$ using 18 MeV protons (14.2 MeV on target) and was separated from [^{18}O]H_2O using a QMA short column (Waters, Milford, MA, USA). [^{18}F]F$^-$ was eluted from the resin with aqueous K_2CO_3 (3.3 mg/0.3 mL) into a vial containing a solution of 4,7,13,16,21,24-hexaoxa-1,10-diazabicyclo[8,8,8]hexacosane (Kryptofix 222, 25 mg) in CH_3CN (1.5 mL) and transferred into another reaction vessel in the hot cell. An aqueous [^{18}F]F$^-$ solution was dried at 120 °C for 15 min to remove H_2O and CH_3CN. Subsequently, trifluoromethanesulfonic acid 2-bromoethyl ester[17] (8 μL) in *o*-dichlorobenzene (0.4 mL) was added to the radioactive mixture. [^{18}F]2-Fluoroethyl bromide in this vessel was distilled under a helium flow (90–100 mL/min) at 130 °C for 5 min and bubbled into another vessel containing the *O*-desmethyl precursor (**5** or **9**; 1.0 mg) and 0.33 M tetrabutylammonium hydroxide in methanol (7 μL) in anhydrous DMF (0.35 mL) at −15 °C, and the reaction mixture was heated and maintained at 120 °C for 10 min. Preparative HPLC purification was performed on a Capcell Pak C18 UG 80 column (10 mm internal diameter × 250 mm length; Shiseido, Tokyo, Japan) using a mobile phase of acetonitrile/water/triethylamine (60:30:0.1, v/v/v, for [^{18}F]**3**; 65:35:0.1, v/v/v, for [^{18}F]**4**) at a flow rate of 3.5 mL/min for [^{18}F]**3** and 5.0 mL/min for [^{18}F]**4**. Retention times of [^{18}F]**3** and [^{18}F]**4** were 10 and 9 min, respectively. HPLC fractions of [^{18}F]**3** or [^{18}F]**4** were collected into a flask to which Tween 80 (75 μL) in ethanol (0.3 mL) had been added before radiosynthesis, and these fractions were then evaporated to dryness. The residue was dissolved in physiological saline.

The products were analyzed by HPLC using a Capcell Pak C18 UG 80 column (4.6 mm internal diameter × 250 mm length; Shiseido). Elution was performed using the same mobile phase as that used for preparative HPLC at a flow rate of 2.0 mL/min. Retention times of [^{18}F]**3** and [^{18}F]**4** were 4.3 and 4.5 min, respectively.

5.5. In vitro accumulation assay

The doxorubicin-resistant human uterus sarcoma cell line (MES-SA/Dx5)[18] was obtained from the American Type Tissue Culture Collection (ATCC, Rockville, MD, USA). Cell lines were grown as a monolayer in McCoy's 5A medium (ATCC) supplemented with

10% fetal calf serum (ATCC) in a humidified atmosphere of 5% CO_2 in air at 37 °C.

MES-SA/Dx5 cells were plated on 24-well plates (105 cells/well) and incubated at 37 °C with complete growth medium in a humidified atmosphere of 5% CO_2. After a monolayer was formed, cells were incubated for 120 min in medium containing 7.4 MBq/ml tracer ([^{18}F]**3** or [^{18}F]**4**) with or without 10 μM one of **1**, **2**, **3** and **4**. After removing the medium, cells were washed five times with pre-chilled phosphate buffered saline and dissolved with 0.2 M NaOH. Radioactivities of cell lysates were measured using the automatic gamma counter (Wizard 3″ 1480; Perkin Elmer, Waltham, MA, USA). After measuring radioactivity, protein concentrations of cell lysates were measured using a DC protein assay kit (Bio-Rad). Accumulation of tracer in MES-SA/Dx5 cells treated with MDR inhibitor was expressed as the percentage of increased accumulation of tracer compared to untreated cells (control cells) using the following formula: percentage of increase = 100 × [percent incubation dose per mg protein in cells (%ICD/mg protein) treated with MDR inhibitor − %ICD/mg protein in the control cells]/%ICD/mg protein in cells treated with MDR inhibitor.[29,30]

5.6. Animals

Animals were maintained and handled in accordance with the recommendations by the US National Institutes of Health and in-house guidelines (National Institute of Radiological Sciences, Chiba, Japan). The animal experiments were approved by the Animal Ethics Committee of the National Institute of Radiological Sciences. Male FVB mice were purchased from CLEA Japan (Tokyo, Japan). Male P-gp knockout [Mdr1a/1b(−/−)],[31] Bcrp knockout [Abcg2 (−/−)][32] and P-gp/Bcrp knockout [Mdr1a/1b(−/−)-Abcg2(−/−)] mice[33] were purchased from Taconic Farm (Hudson, NY, USA).

5.7. Biodistribution in mice

Tissue distribution of radioactivity after injection of [^{18}F]**3** and [^{18}F]**4** were investigated. [^{18}F]**3** or [^{18}F]**4** (1.0–4.8 MBq/7.1–34 pmol) was intravenously injected in normal FVB mice (age, 8–10 weeks; weight, 25–29 g). Mice were sacrificed by cervical dislocation at 5, 15, 30, 60, or 90 min after injection (n = 4 per group).

Inhibitory effects of the function of drug efflux transporters on tissue distribution of [^{18}F]**3** and [^{18}F]**4** were investigated. [^{18}F]**3** or [^{18}F]**4** (1.0–4.8 MBq/7.1–34 pmol) was intravenously co-injected with or without **1** (5 mg/kg) in normal FVB mice (age, 8–10 weeks; weight, 25–29 g). Mice were sacrificed by cervical dislocation at 30 min after injection (n = 4 per group).

Blood samples were collected by heart puncture, and the tissues were dissected and weighed. Radioactivity in samples was measured using the automatic gamma counter. Radioactivity level was decay corrected to injection time and was expressed as the percentage of injected radioactivity per gram of tissue (%ID/g).

5.8. Metabolite analysis in the brain and plasma of mice

[^{18}F]**3** (17–29 MBq/0.12–0.21 nmol) or [^{18}F]**4** (9–36 MBq/0.064–0.26 nmol) was intravenously co-injected with **1** (5 mg/kg) into normal FVB mice (age, 9–13 weeks; weight, 24–31 g; n = 3–4 per group). Mice were sacrificed by cervical dislocation at 30 and 60 min after injection. Blood samples were collected into a heparinized syringe by heart puncture, and the whole brain was dissected out. Deproteinization was performed using previously described methods mentioned below.[34] Plasma and homogenized brain tissues were deproteinized with the same volume of ice-cold acetonitrile. The mixture was then vortexed and centrifuged at 20,000g for 2 min, and the supernatant was collected. Supernatants were analyzed by HPLC using a radioactivity detector[35] and an ultraviolet detector at 254 nm on a Novapak C18 column (8 mm internal diameter × 100 mm length; Waters) contained within a radial compression module (RCM-100, Waters). Elution was performed using a mixture of acetonitrile and 0.1 M sodium acetate buffer (pH 4.7) (45:55, v/v, for [^{18}F]**3**; 50:50, v/v, for [^{18}F]**4**) at a flow rate of 2.0 mL/min. Retention times of [^{18}F]**3** and [^{18}F]**4** were 5.6 and 5.7 min, respectively. Radioactivity in the supernatants, residual precipitates after centrifugation, and waste solution from HPLC were measured using the automatic gamma counter. Percentages of unchanged form were then determined.

5.9. PET study in mice

PET scans were obtained using an Inveon Dedicated PET Scanner (Siemens Medical Solutions, Knoxville, TN, USA). P-gp/Bcrp knockout mice (age, 16–26 weeks; weight, 29–36 g), P-gp knockout mice (age, 18–39 weeks; weight, 27–37 g), Bcrp knockout mice (age, 18–39 weeks; weight, 26–36 g) and wild-type mice (age, 7–22 weeks; weight, 23–35 g) were used in the PET study.

Mice were anesthetized with isoflurane (1.0–1.5%, v/v) and placed in a prone position on the bed. [^{18}F]**3** (3.7–5.4 MBq/26–39 pmol) or [^{18}F]**4** (2.8–5.6 MBq/20–40 pmol) was intravenously co-injected with or without **1** (5 mg/kg) in mice (n = 4–6 per group). A time-sequential scan was performed for 60 min in the three-dimensional (3D) list mode with an energy window of 350–650 keV. List-mode data were sorted into 3D sinograms (6 × 10 s, 4 × 15 s, 5 × 1 min, 4 × 2 min, 3 × 5 min, and 3 × 10 min), which were then Fourier rebinned into two-dimensional sinograms. Dynamic images were reconstructed with filtered back projection using a ramp filter. Decay-corrected radioactivity was expressed as SUV, (tissue radioactivity/milliliter of tissue)/(injected radioactivity/gram of body weight)]. ROIs were masked on the brain using the ASIPro VM software (Siemens Medical Solutions). ROIs in the blood were masked on the ventricular cavity using the frame of first 5 seconds after the administration. AUC of ROIs in the brain (AUC_{brain}, SUV min) was calculated starting from 0 to 60 min.

5.10. Statistical analysis

Quantitative data are expressed as the mean ± standard deviation (SD). In the in vitro accumulation assay and in vivo distribution study, differences between control and treatment groups were determined by one-way analysis of variance (ANOVA) and Dunnett's post hoc tests. In metabolite analysis and PET study, differences between all pairs of groups were determined by one-way ANOVA and Bonferroni's multiple comparison tests. Data was analyzed using the GraphPad Prism 5 software (GraphPad Software, San Diego, CA, USA). Differences were considered significant if P <0.05.

Acknowledgments

We are grateful to the staff of Cyclotron Operation Section NIRS for their technical assistance in radioisotope production, and the staff of the Department of Molecular Probes NIRS for their assistance.

Supplementary data

Supplementary data (the purity of **3** and **4** was determined by HPLC) associated with this article can be found, in the online version, at doi:10.1016/j.bmc.2010.12.004.

References and notes

1. Ayrton, A.; Morgan, P. *Xenobiotica* **2001**, *31*, 469.
2. Borst, P.; Elferink, R. O. *Annu. Rev. Biochem.* **2002**, *71*, 537.
3. Schinkel, A. H.; Jonker, J. W. *Adv. Drug Deliv. Rev.* **2003**, *55*, 3.

4. Löscher, W.; Potschka, H. *Prog. Neurobiol.* **2005**, *76*, 22.
5. Gottesman, M. M.; Fojo, T.; Bates, S. E. *Nat. Rev. Cancer* **2002**, *2*, 48.
6. Hyafil, F.; Vergely, C.; Du Vignaud, P.; Grand-Perret, T. *Cancer Res.* **1993**, *53*, 4595.
7. Roe, M.; Folkes, A.; Ashworth, P.; Brumwell, J.; Chima, L.; Hunjan, S.; Pretswell, I.; Dangerfield, W.; Ryder, H.; Charlton, P. *Bioorg. Med. Chem. Lett.* **1999**, *9*, 595.
8. de Bruin, M.; Miyake, K.; Litman, T.; Robey, R.; Bates, S. E. *Cancer Lett.* **1999**, *146*, 117.
9. Allen, J. D.; Brinkhuis, R. F.; Wijnholds, J.; Schinkel, A. H. *Cancer Res.* **1999**, *59*, 4237.
10. Martin, C.; Berridge, G.; Mistry, P.; Higgins, C.; Charlton, P.; Callaghan, R. *Br. J. Pharmacol.* **1999**, *128*, 403.
11. Pick, A.; Müller, H.; Wiese, M. *Bioorg. Med. Chem.* **2008**, *16*, 8224.
12. Dörner, B.; Kuntner, C.; Bankstahl, J. P.; Bankstahl, M.; Stanek, J.; Wanek, T.; Stundner, G.; Mairinger, S.; Löscher, W.; Müller, M.; Langer, O.; Erker, T. *J. Med. Chem.* **2009**, *52*, 6073.
13. Kawamura, K.; Yamasaki, T.; Konno, F.; Yui, J.; Hatori, A.; Yanamoto, K.; Wakizaka, H.; Takei, M.; Kimura, Y.; Fukumura, T.; Zhang, M.-R. *Mol. Imaging Biol.* **2010**. doi:10.1007/s11307-010-0313-1.
14. Kawamura, K.; Konno, F.; Yui, J.; Yamasaki, T.; Hatori, A.; Yanamoto, K.; Wakizaka, H.; Takei, M.; Nengaki, N.; Fukumura, T.; Zhang, M.-R. *Ann. Nucl. Med.* **2010**, *24*, 403.
15. Bauer, F.; Kuntner, C.; Bankstahl, J. P.; Wanek, T.; Bankstahl, M.; Stanek, J.; Mairinger, S.; Dörner, B.; Löscher, W.; Müller, M.; Erker, T.; Langer, O. *Bioorg. Med. Chem.* **2010**, *18*, 5489.
16. Fukumura, T.; Suzuki, H.; Mukai, K.; Zhang, M.-R.; Yoshida, Y.; Nemoto, K.; Suzuki, K. *J. Labelled Compd. Radiopharm.* **2007**, *50*, S202.
17. Zhang, M.-R.; Tsuchiyama, A.; Haradahira, T.; Yoshida, Y.; Furutsuka, K.; Suzuki, K. *Appl. Radiat. Isot.* **2002**, *57*, 335.
18. Harker, W. G.; Sikic, B. I. *Cancer Res.* **1985**, *45*, 4091.
19. Koo, J. S.; Choi, W. C.; Rhee, Y. H.; Lee, H. J.; Lee, E. O.; Ahn, K. S.; Bae, H. S.; Ahn, K. S.; Kang, J. M.; Choi, S. U.; Kim, M. O.; Lu, J.; Kim, S. H. *Life Sci.* **2008**, *83*, 700.
20. Wu, G.; Liu, J.; Bi, L.; Zhao, M.; Wang, C.; Michèle, B.-F.; Ju, J.; Peng, F. *Tetrahedron* **2007**, *63*, 5510.
21. de Vries, N. A.; Zhao, J.; Kroon, E.; Buckle, T.; Beijnen, J. H.; van Tellingen, O. *Clin. Cancer Res.* **2007**, *13*, 6440.
22. Kannan, P.; Brimacombe, K. R.; Zoghbi, S. S.; Liow, J. S.; Morse, C.; Taku, A. K.; Pike, V. W.; Halldin, C.; Innis, R. B.; Gottesman, M. M.; Hall, M. D. *Drug Metab. Dispos.* **2010**, *38*, 917.
23. Luurtsema, G.; Schuit, R. C.; Klok, R. P.; Verbeek, J.; Leysen, J. E.; Lammertsma, A. A.; Windhorst, A. D. *Nucl. Med. Biol.* **2009**, *36*, 643.
24. Cisternino, S.; Mercier, C.; Bourasset, F.; Roux, F.; Scherrmann, J. M. *Cancer Res.* **2004**, *64*, 3296.
25. Zhou, L.; Schmidt, K.; Nelson, F. R.; Zelesky, V.; Troutman, M. D.; Feng, B. *Drug Metab. Dispos.* **2009**, *37*, 946.
26. Pike, V. W. P. E. T. *Trends Pharmacol. Sci.* **2009**, *30*, 431.
27. Dodic, N.; Dumaitre, B.; Daugan, A.; Pianetti, P. *J. Med. Chem.* **1995**, *38*, 2418.
28. Gilday, J. P.; Moody, D. PCT. Int. Appl. WO/2004/024703 A1, 2004.
29. Yamasaki, T.; Kumata, K.; Yanamoto, K.; Hatori, A.; Takei, M.; Nakamura, Y.; Koike, S.; Ando, K.; Suzuki, K.; Zhang, M.-R. *Nucl. Med. Biol.* **2009**, *36*, 801.
30. Angelini, A.; Iezzi, M.; Di Febbo, C.; Di Ilio, C.; Cuccurullo, F.; Porreca, E. *Oncol. Rep.* **2008**, *20*, 731.
31. Schinkel, A. H.; Mayer, U.; Wagenaar, E.; Mol, C. A.; van Deemter, L.; Smit, J. J.; van der Valk, M. A.; Voordouw, A. C.; Spits, H.; van Tellingen, O.; Zijlmans, J. M.; Fibbe, W. E.; Borst, P. *Proc. Natl. Acad. Sci. U.S.A.* **1997**, *94*, 4028.
32. Jonker, J. W.; Buitelaar, M.; Wagenaar, E.; Van Der Valk, M. A.; Scheffer, G. L.; Scheper, R. J.; Plosch, T.; Kuipers, F.; Elferink, R. P.; Rosing, H.; Beijnen, J. H.; Schinkel, A. H. *Proc. Natl. Acad. Sci. U.S.A.* **2002**, *99*, 15649.
33. Jonker, J. W.; Freeman, J.; Bolscher, E.; Musters, S.; Alvi, A.; Titley, I. *Stem Cells* **2005**, *23*, 1059.
34. Kawamura, K.; Yamasaki, T.; Yui, J.; Hatori, A.; Konno, F.; Kumata, K.; Irie, T.; Fukumura, T.; Suzuki, K.; Kanno, I.; Zhang, M.-R. *Nucl. Med. Biol.* **2009**, *36*, 239.
35. Takei, M.; Kida, T.; Suzuki, K. *Appl. Radiat. Isot.* **2001**, *55*, 229.